

A High-Resolution Method for Quantum Confinement Transport Simulations in MOSFETs

Shinji Odanaka, *Senior Member, IEEE*

Abstract—This paper describes a new discretization scheme for quantum confinement transport simulations using a quantum drift–diffusion model. A high-resolution scheme is constructed by developing an exponential-fitting method with the slope limiter in a class of conservative schemes to simulate the flow of electrons with quantum confinement effects in MOSFETs. This method is reinterpreted as a flux-limiter method that hybridizes a low-order flux and a high-order flux into a single numerical flux. The discretization method provides good approximations to the density profile in the smooth regions and boundary layers of the electron flow and allows high-resolution simulations of quantum confinement transport in ultrasmall MOSFETs.

Index Terms—Numerical analysis, partial differential equation, quantum theory, semiconductor device model, simulation.

I. INTRODUCTION

THE performance of ultrasmall MOSFETs available for the future integrated system relies on quantum confinement transport in narrow gate- or thin body-induced channels [1], [2]. For the modeling of such MOS transport, the quantum drift–diffusion (QDD) model, which is also called the density-gradient model, has been introduced as a quantum-corrected version of the classical drift–diffusion model with $O(\hbar^2)$ corrections to the stress tensor [3]. This model is a fluid dynamical form of the Schrödinger equation and viewed as one of the hierarchies of the quantum hydrodynamic models, which is derived from a moment expansion of the Wigner–Boltzmann equation adding a collision term [4]. The $O(\hbar^2)$ terms of the QDD model allow quantum confinement transport simulations in MOSFETs and represent the smooth regions and boundary layers of the electron flow in the channels. Nonlinear discretization schemes have been proposed for numerical approximation of solutions to the QDD equation [5]–[7] to achieve high computational capability of electrical characteristics. Recently, Tang *et al.* [8] pointed out that the numerical solutions obtained by a nonlinear discretization scheme, which is developed in [5] and [6], are sensitive to the boundary conditions at the silicon/oxide interface while giving high accuracy in smooth regions of the flow [8]. This is a major concern to achieve good approximations to the flow of electrons with quantum confinement effects.

In this paper, we describe a high-resolution method for quantum confinement transport simulations in MOSFETs on the basis of our previous work [7], which provides a general

procedure that produces low-order and high-order conservative schemes to the QDD equation. A high-resolution scheme is constructed by developing an exponential-fitting method with the slope limiter in a class of conservative schemes. The discretization scheme is evaluated for carrier transport simulations with quantum confinement effects in a MOSFET. The spurious profile arising in the boundary layer is suppressed by the new discretization method. Section II discusses a QDD model for numerical simulations of quantum confinement transport. Section III describes a new discretization scheme to the stationary QDD equations, which is constructed by an exponential-fitting method with the slope limiter. This method is reinterpreted as a flux-limiter method that hybridizes a low-order flux and a high-order flux into a single numerical flux. In Section IV, the slope limiter for the new discretization scheme is designed by numerical experiments. The resulting scheme is validated in the electron density distributions of a MOSFET, comparing with those calculated from the Schrödinger equation coupling with Poisson equation.

II. QDD MODEL

The QDD model is derived as a quantum-corrected version of the classical drift–diffusion model, introducing the generalized chemical potential form that is related to the density and its gradient [9]. Assuming Boltzmann statistics, the generalized chemical potentials φ_n and φ_p are written as

$$\varphi_n = \varphi - \frac{kT}{q} \ln \left(\frac{n}{n_i} \right) + \gamma_n \quad (1)$$

and

$$\varphi_p = \varphi + \frac{kT}{q} \ln \left(\frac{p}{n_i} \right) - \gamma_p \quad (2)$$

where n and p are the electron and hole densities, φ is the electrostatic potential, n_i is the intrinsic density, k is the Boltzmann's constant, q is the electronic charge, and T is the carrier temperature. A form of the quantum potentials γ_n and γ_p in terms of the electrons and holes was derived from $O(\hbar^2)$ corrections to the stress tensor [3], i.e.,

$$\gamma_n = 2b_n \frac{\nabla^2 \sqrt{n}}{\sqrt{n}} \quad (3)$$

$$\gamma_p = 2b_p \frac{\nabla^2 \sqrt{p}}{\sqrt{p}}. \quad (4)$$

Manuscript received October 28, 2005; revised January 28, 2006 and April 21, 2006. This paper was recommended by Associate Editor H. Kosina.

The author is with the Computer Assisted Science Division, Cybermedia Center, Osaka University, Osaka 560-0043, Japan.

Digital Object Identifier 10.1109/TCAD.2006.882531

The density-gradient coefficients for electrons and holes were identified by $b_n = \hbar^2/(12qm_n^*)$ and $b_p = \hbar^2/(12qm_p^*)$, respectively, where m_n^* and m_p^* are effective masses for the electrons and holes, respectively, and \hbar is the Planck's constant. In this case, the form of the quantum potential is different by a factor of 1/3 from the Bohm potential [10].

The governing equations for the electrons and holes in a semiconductor then become

$$\varepsilon \Delta \varphi = q(n - p + N) \quad (5)$$

$$-2b_n \nabla^2 S_n + \gamma_n S_n = 0 \quad (6)$$

$$\nabla(\mu_n n \nabla \varphi_n) + R = 0 \quad (7)$$

$$-2b_p \nabla^2 S_p + \gamma_p S_p = 0 \quad (8)$$

$$-\nabla(\mu_p p \nabla \varphi_p) + R = 0 \quad (9)$$

where ε is the electric permittivity, μ_n and μ_p are electron and hole mobilities, respectively, N is the ionized impurity density, and R is the recombination rate. S_n and S_p are the root densities \sqrt{n} and \sqrt{p} , respectively. By introducing the generalized chemical potentials, the current continuity equations for the electrons and holes are split into the two second-order differential equations, respectively. In a simulation region Ω , the QDD equations are solved, supplementing appropriate boundary conditions on a boundary $\partial\Omega$.

In our previous work [7], we constructed a multidimensional discretization scheme to the QDD equations, employing an exponential transformation of the root densities $S_n = \sqrt{n_i} e^u$ and $S_p = \sqrt{p_i} e^v$, where $u = (\varphi + \gamma_n - \varphi_n)/2$ and $v = (\varphi_p + \gamma_p - \varphi)/2$, respectively. To achieve a numerical advantage, (6) was replaced by the equivalent form

$$-b_n \nabla(S_n \nabla u) + S_n u = \frac{S_n}{2} (\varphi - \varphi_n) \quad (10)$$

where all of potentials are scaled by the Boltzmann voltage. A similar expression is obtained for the holes. The nonlinear equation is solved subject to the boundary conditions for the potential u . As a result, it is possible to ensure the positivity of the root density S_n by the uniform bound on the solution of (10). The boundary condition at contacts is given by $u = \varphi_b/2$, assuming $\gamma_n = 0$ at ohmic contacts, where φ_b is the built-in voltage. At open boundaries, the normal derivative vanishes, i.e., $\partial u / \partial \nu = 0$. The boundary condition of u on the silicon/oxide interface is given by a small but nonzero value of the carrier density. The zero value of the carriers at the interface is incompatible with the Boltzmann statistics. In fact, this condition requires the potential u at the interface to tend to $-\infty$ when the Boltzmann statistics is assumed.

III. HIGH-RESOLUTION SCHEME

The discretization of the QDD equation is performed for (7) and (10), applying the finite-volume method to construct a multidimensional scheme [7]. The numerical method developed in [7] provides a general procedure that produces low-order and high-order nonlinear schemes to the QDD equation.

Assuming that the flux $F = S_n \nabla u$ in (10), we obtain by Green's formula over each computational cell $\Omega_{i,j}$ that

$$\int_{\partial\Omega_{i,j}} b_n S_n \frac{\partial u}{\partial \nu} ds - \int_{\Omega_{i,j}} S_n u dx = -\frac{1}{2} \int_{\Omega_{i,j}} S_n (\varphi - \varphi_n) dx \quad (11)$$

where the simulation region Ω is partitioned into computational cells $\Omega_{i,j}$, i.e., $\Omega = \cup \Omega_{i,j}$. ν denotes the unit outward normal to the boundary $\partial\Omega_{i,j}$ of the computational cell. In a staggered Cartesian grid in two dimensions, where the computational cell is rectangular, and the variables φ , φ_n , u , and S_n are defined at cell centers and the numerical flux F is defined at cell interfaces, we obtain a discrete form of (11), i.e.,

$$\begin{aligned} & a_j b_n (F_{i+1/2,j} - F_{i-1/2,j}) \\ & + a_i b_n (F_{i,j+1/2} - F_{i,j-1/2}) - u_{i,j} \int_{y_{j-1/2}}^{y_{j+1/2}} \int_{x_{i-1/2}}^{x_{i+1/2}} S_n dx \\ & = -\frac{1}{2} (\varphi - \varphi_n)_{i,j} \int_{y_{j-1/2}}^{y_{j+1/2}} \int_{x_{i-1/2}}^{x_{i+1/2}} S_n dx \end{aligned} \quad (12)$$

where a_i and a_j are the cell sizes of the computational cell $\Omega_{i,j}$. To find $F_{i+1/2,j}$ at cell interfaces, integrating the flux F over the interval $[x_i, x_{i+1}]$, an approximation $F_{i+1/2,j}$ yields

$$F_{i+1/2,j} = \frac{u_{i+1,j} - u_{i,j}}{\int_{x_i}^{x_{i+1}} \frac{dx}{S_n}}. \quad (13)$$

A similar expression is obtained for $F_{i-1/2,j}$, $F_{i,j-1/2}$, and $F_{i,j+1/2}$. Substituting in (12) the average fluxes $F_{i\pm 1/2,j}$ and $F_{i,j\pm 1/2}$ leads to a class of conservative schemes [11].

In this case, the accuracy of the numerical flux depends on the explicit integration of the function S_n in (13), i.e.,

$$\int_{x_i}^{x_{i+1}} \frac{dx}{S_n} = \int_{x_i}^{x_{i+1}} e^{-u} dx \quad (14)$$

and hence the explicit integration method for the function S_n leads to a procedure that produces low-order and high-order conservative schemes.

The piecewise constant representation of the potential u on the interval $[x_i, x_{i+1}]$ leads to a low-order flux F_L at the cell interfaces. By interpolating linearly between the two grids, the low-order flux F_L is expressed as

$$\begin{aligned} F_L &= \frac{1}{h_{i+1}} \exp\left(\frac{u_{i+1,j} + u_{i,j}}{2}\right) (u_{i+1,j} - u_{i,j}) \\ &= \frac{1}{h_{i+1}} \sqrt{S_{ni+1,j} S_{ni,j}} (u_{i+1,j} - u_{i,j}) \\ &= \frac{1}{h_{i+1}} \sqrt{S_{ni+1,j} / S_{ni,j}} \\ &\quad \times B(\ln(S_{ni+1,j} / S_{ni,j})) (S_{ni+1,j} - S_{ni,j}) \end{aligned} \quad (15)$$

where $h_{i+1} = x_{i+1} - x_i$. $B(\cdot)$ is the Bernoulli function. A similar expression is obtained by taking $i - 1$, $j - 1$, and $j + 1$. A substitution of the numerical fluxes F_L into (12) results in a low-order nonlinear scheme, which corresponds to a nonlinear scheme developed in [5] and [6] if the numerical flux is rewritten in terms of the root density S_n [7]. For constructing high-order schemes, we can approximate the numerical flux by the piecewise-linear representation of u on the interval $[x_i, x_{i+1}]$, assuming that du/dx is constant on the interval $[x_i, x_{i+1}]$, i.e.,

$$u = \frac{u_{i+1,j} + u_{i,j}}{2} + \sigma_{i+1,j}^x \left(x - \frac{x_{i+1} + x_i}{2} \right). \quad (16)$$

If we make the natural choice

$$\sigma_{i+1,j}^x = \frac{u_{i+1,j} - u_{i,j}}{h_{i+1}} \quad (17)$$

then the method results in a high-order numerical flux described in [7], i.e.,

$$F_H = \frac{1}{h_{i+1}} \exp(u_{i+1,j}) B(u_{i+1,j} - u_{i,j}) (u_{i+1,j} - u_{i,j}). \quad (18)$$

Substituting in (12) the high-order fluxes yields a high-order nonlinear scheme developed in [7]. The piecewise-linear representation of u on the interval leads to an extension of the Scharfetter–Gummel approach [12] to the QDD equation [7]. If we further limit the slope (17), i.e.,

$$\sigma_{i+1,j}^x = \frac{u_{i+1,j} - u_{i,j}}{h_{i+1}} \theta_{i+1,j}^x \quad (19)$$

then we obtain a more general discrete form for the numerical flux as follows:

$$F_{i+1/2,j} = \frac{1}{h_{i+1}} \exp \left(\frac{(1 + \theta_{i+1,j}^x) u_{i+1,j} + (1 - \theta_{i+1,j}^x) u_{i,j}}{2} \right) \times B((u_{i+1,j} - u_{i,j}) \theta_{i+1,j}^x) (u_{i+1,j} - u_{i,j}). \quad (20)$$

A similar expression is obtained for $F_{i-1/2,j}$, $F_{i,j-1/2}$, and $F_{i,j+1/2}$. It is worth while noting that the numerical flux is

$$F_{i+1/2,j} = \begin{cases} F_L, & \text{if } \theta_{i+1,j}^x = 0 \\ F_H, & \text{if } \theta_{i+1,j}^x = 1. \end{cases} \quad (21)$$

The numerical flux at the silicon/oxide interface is written as

$$F_B = \frac{2}{h_{i+1}} \exp \left(\frac{(1 + \theta_{i+1,j}^x) u_B + (1 - \theta_{i+1,j}^x) u_{i,j}}{2} \right) \times B((u_B - u_{i,j}) \theta_{i+1,j}^x) (u_B - u_{i,j}) \quad (22)$$

where the boundary potential $u_B = (1/2) \ln(n_B/n_i)$, which is scaled by the Boltzmann voltage, is given by a small but

nonzero value of the root density $\sqrt{n_B} = \sqrt{n_i} e^{u_B}$ at the silicon/oxide interface.

An average of S_n in each computational cell is performed by integrating the piecewise-linear representation of u by

$$u = u_{i,j} + \frac{\partial u}{\partial x} (x - x_i) + \frac{\partial u}{\partial y} (y - y_j) \quad (23)$$

where $\partial u / \partial x = \text{const}$ on the intervals $[x_{i-1/2}, x_i]$ and $[x_i, x_{i+1/2}]$, and $\partial u / \partial y = \text{const}$ on the intervals $[y_{j-1/2}, y_j]$ and $[y_j, y_{j+1/2}]$, respectively. Then, after some calculation, we have the following approximation:

$$\Lambda_{i,j} = \int_{y_{j-1/2}}^{y_{j+1/2}} \int_{x_{i-1/2}}^{x_{i+1/2}} S_n dx = \frac{1}{4} e^{u_{i,j}} \left(\frac{h_i}{B\left(\frac{u_{i-1,j} - u_{i,j}}{2}\right)} + \frac{h_{i+1}}{B\left(\frac{u_{i+1,j} - u_{i,j}}{2}\right)} \right) \cdot \left(\frac{h_j}{B\left(\frac{u_{i,j} - u_{i,j-1}}{2}\right)} + \frac{h_{j+1}}{B\left(\frac{u_{i,j+1} - u_{i,j}}{2}\right)} \right). \quad (24)$$

Substituting (20) and (24) into (12), we obtain a new nonlinear scheme to (10) subject to the boundary conditions for u , i.e.,

$$\begin{aligned} & \frac{a_j}{h_{i+1}} b_n \exp \left(\frac{(1 + \theta_{i+1,j}^x) u_{i+1,j} + (1 - \theta_{i+1,j}^x) u_{i,j}}{2} \right) \\ & \times B((u_{i+1,j} - u_{i,j}) \theta_{i+1,j}^x) (u_{i+1,j} - u_{i,j}) \\ & - \frac{a_j}{h_i} b_n \exp \left(\frac{(1 + \theta_{i,j}^x) u_{i,j} + (1 - \theta_{i,j}^x) u_{i-1,j}}{2} \right) \\ & \times B((u_{i,j} - u_{i-1,j}) \theta_{i,j}^x) (u_{i,j} - u_{i-1,j}) \\ & + \frac{a_i}{h_{j+1}} b_n \exp \left(\frac{(1 + \theta_{i,j+1}^y) u_{i,j+1} + (1 - \theta_{i,j+1}^y) u_{i,j}}{2} \right) \\ & \times B((u_{i,j+1} - u_{i,j}) \theta_{i,j+1}^y) (u_{i,j+1} - u_{i,j}) \\ & - \frac{a_i}{h_j} b_n \exp \left(\frac{(1 + \theta_{i,j}^y) u_{i,j} + (1 - \theta_{i,j}^y) u_{i,j-1}}{2} \right) \\ & \times B((u_{i,j} - u_{i,j-1}) \theta_{i,j}^y) (u_{i,j} - u_{i,j-1}) \\ & - \Lambda_{i,j} u_{i,j} = -\frac{\Lambda_{i,j}}{2} (\varphi - \varphi_n)_{i,j}. \end{aligned} \quad (25)$$

The parameter θ can be considered as a slope limiter that produces low-order and high-order schemes to the QDD equation automatically. This approach leads to a new numerical method, i.e., an exponential-fitting method with the slope limiter. The slope-limiter method has been introduced in the computational

fluid dynamics as shock-capturing algorithms that produce high-order accuracy on smooth solutions and sharp resolution in the vicinity of steep gradients [13]. This method is reinterpreted as a flux-limiter method, which hybridizes a low-order flux and a high-order flux into a single flux [13].

The exponential-fitting method with the slope limiter is also viewed as a flux-limiter method that hybridizes a low-order flux and a high-order flux into a single flux. Expanding the Bernoulli function and the exponential function in a Taylor series with respect to $u_{i+1,j} - u_{i,j}$, we find from (20) that

$$F_{i+1/2,j} = F_L + \theta_{i+1,j}^x (F_H - F_L) + O(|u_{i+1,j} - u_{i,j}|^2). \quad (26)$$

This means that the slope limiter θ represents the flux limiter.

In a previous work [8], Tang *et al.* pointed out that the results obtained by a nonlinear scheme [5], [6], which is derived from the low-order flux in terms of the root density S_n (15), are sensitive to the boundary conditions given by the extremely small carrier density at the silicon/oxide interface [8]. Applying the analysis of the problem, they proposed a mixed-difference scheme in which the standard linear scheme is used in the boundary layer ($x \leq 0.5$ nm at the depth direction) and the nonlinear scheme in the smooth regions in the channel [8]. The numerical scheme (25) developed here hybridizes low-order and high-order schemes in terms of the potential u , which are derived from (15) and (18). Although both schemes are nonlinear, it is expected that a high-order scheme works well in smooth regions of the electron flow, and a low-order scheme behaves well near the silicon/oxide interface. In the numerical scheme (25), the slope limiter θ should be near zero in the boundary layer, whereas in the smooth regions of the flow, we want θ to be 1. Then, the numerical flux F reduces to the low-order flux F_L near the silicon/oxide interface and to the high-order flux F_H in smooth regions in the channel automatically. The actual hybridization between F_L and F_H requires a way for choosing the slope-limiter function. It is possible to construct some function for the slope limiter by numerical experiments, as will be mentioned later.

For the discretization of the current continuity equation, (7) is rewritten in terms of the Slotboom variable $\eta = n_i \exp(-\varphi_n)$ for the generalized chemical potential as

$$-\nabla(\mu_n e^{\Phi} \nabla \eta) + R = 0 \quad (27)$$

where $\Phi = \varphi + \gamma_n$. The current density $J = \mu_n e^{\Phi} \nabla \eta$ is discretized in terms of the electron density, i.e.,

$$\begin{aligned} J_{i+1/2,j} &= \mu_{n_{i+1/2,j}} \frac{\eta_{i+1,j} - \eta_{i,j}}{\int_{x_i}^{x_{i+1}} e^{-\Phi} dx} \\ &= \frac{\mu_{n_{i+1/2,j}}}{h_{i+1}} (B(\Phi_{i+1,j} - \Phi_{i,j})n_{i+1,j} \\ &\quad - B(\Phi_{i,j} - \Phi_{i+1,j})n_{i,j}). \end{aligned} \quad (28)$$

This approach leads to the well-known Scharfetter–Gummel scheme [12], i.e.,

$$\begin{aligned} &\frac{a_j}{h_{i+1}} \mu_{n_{i+1/2,j}} (B(\Phi_{i+1,j} - \Phi_{i,j})n_{i+1,j} \\ &\quad - B(\Phi_{i,j} - \Phi_{i+1,j})n_{i,j}) \\ &- \frac{a_j}{h_i} \mu_{n_{i-1/2,j}} (B(\Phi_{i,j} - \Phi_{i-1,j})n_{i,j} \\ &\quad - B(\Phi_{i-1,j} - \Phi_{i,j})n_{i-1,j}) \\ &+ \frac{a_i}{h_{j+1}} \mu_{n_{i,j+1/2}} (B(\Phi_{i,j+1} - \Phi_{i,j})n_{i,j+1} \\ &\quad - B(\Phi_{i,j} - \Phi_{i,j+1})n_{i,j}) \\ &- \frac{a_i}{h_j} \mu_{n_{i,j-1/2}} (B(\Phi_{i,j} - \Phi_{i,j-1})n_{i,j} \\ &\quad - B(\Phi_{i,j-1} - \Phi_{i,j})n_{i,j-1}) \\ &= \text{vol}(\Omega_{i,j}) R_{i,j}. \end{aligned} \quad (29)$$

Finally, we obtain the full discretization schemes (25) and (29) to the QDD equation.

IV. SIMULATION RESULTS FOR MOSFETS

The slope limiter for the numerical scheme (25) is designed by numerical experiments, and the corresponding scheme was validated in the electron density distributions of a MOSFET having thin gate oxide thickness of 1.5 nm and high substrate concentration of $1.0 \times 10^{18} \text{ cm}^{-3}$. The results are compared with those calculated from the Schrödinger–Poisson system including 30 subbands. For the simulations, the value of effective mass is given by a single parameter $m_n^* = 0.26m_0$. The nonuniform grid spacing is adapted to the location of boundaries. The boundary data u_B at the silicon/oxide interface is given by the root density $\sqrt{n_B} = \sqrt{n_i} e^{u_B}$.

We can look at the dependence of the electron density on the boundary data at the silicon/oxide interface to design the slope-limiter functions. Fig. 1 shows the electron density distributions obtained by the high-order nonlinear scheme with different boundary conditions at the silicon/oxide interface. The dependence of the electron density on the boundary data similar to that Tang *et al.* reported in [8] is also represented in the high-order nonlinear scheme. When the boundary condition at the silicon/oxide interface is given by the small carrier density with $\sqrt{n_B} \leq \sqrt{10n_i}$, the incompatible boundary condition induces the spurious profile arising in the singular boundary layer. If the carrier density more than $10\sqrt{n_i}$ at the silicon/oxide interface is given, the high-order nonlinear scheme gives good approximations to the electron density distributions. The dependence of the density profile on the grid spacing adjacent to the silicon/oxide interface is shown in Fig. 2. Although the spurious profile is improved by minimizing the cell size adjacent to the silicon/oxide interface, the discrepancy of the density profile remains in the boundary layer. Fig. 3 shows the electron density distributions calculated using the low-order nonlinear scheme with different boundary conditions. The low-order scheme works well in simulating the electron density

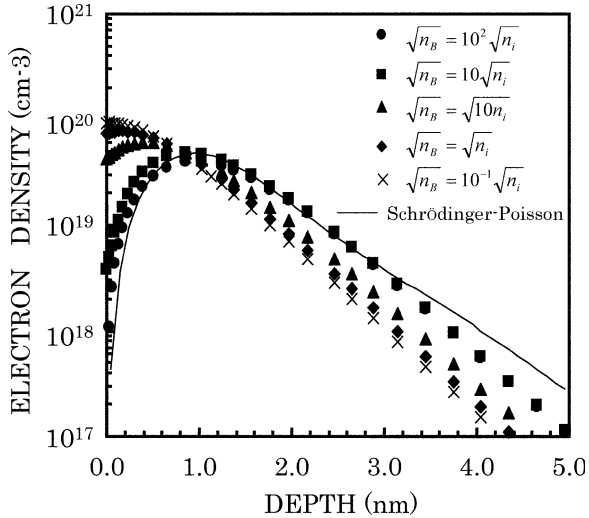


Fig. 1. Electron density distributions calculated using the high-order scheme with different boundary conditions for a MOSFET having 1.5-nm gate oxide thickness and uniform channel doping of $1.0 \times 10^{18} \text{ cm}^{-3}$. The root densities, which give the boundary condition at the silicon/oxide interface, are plotted.

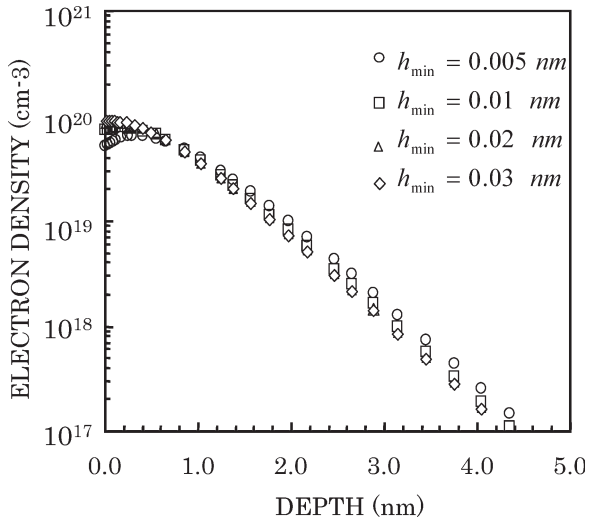


Fig. 2. Electron density distributions calculated using the high-order scheme with different values of the grid spacing h_{\min} adjacent to the silicon/oxide interface.

distributions subject to the boundary condition given by the small but not extremely small value of the electron density with $10^{-1}\sqrt{n_i} \leq \sqrt{n_B} \leq \sqrt{10n_i}$ at the silicon/oxide interface. At the boundary condition given by the relatively large electron density more than $10\sqrt{n_i}$, however, it is further found that the low-order scheme gives poor convergence and poor accuracy in smooth regions of the electron density distributions.

One simple and effective choice of slopes satisfying these results is to define a limiter function on the silicon/oxide interface as

$$\theta(\omega) = \begin{cases} 0, & \text{if } \omega \leq 0 \\ \omega, & \text{if } 0 < \omega < 1 \\ 1, & \text{if } \omega \geq 1 \end{cases} \\ = \max(0, \min(1, \omega)) \quad (30)$$

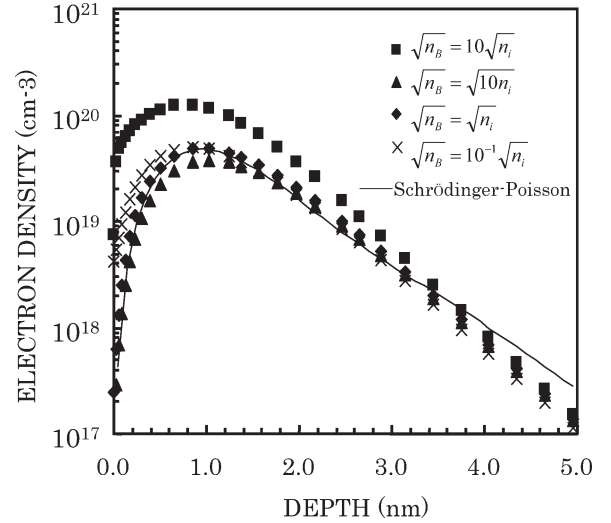


Fig. 3. Electron density distributions calculated using the low-order scheme with different boundary conditions for the same device as shown in Fig. 1. The root densities, which give the boundary condition at the silicon/oxide interface, are plotted.

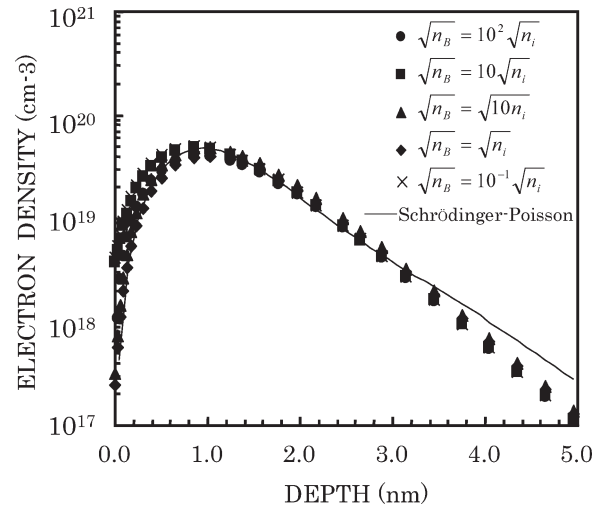


Fig. 4. Electron density distributions calculated using the new discretization scheme with different boundary conditions. The root densities, which give the boundary condition at the silicon/oxide interface, are plotted.

where $\omega = u_B/C$. C is a constant value of $\ln 10$. When $\omega = 1$, the boundary data $u_B = C$, scaled by the Boltzmann voltage, is given by $\sqrt{n_B} = 10\sqrt{n_i}$. In other simulation region, we set the slope limiter θ to 1, and hence, the high-order scheme is used.

The results calculated by the new scheme (25) with the slope-limiter function mentioned above are shown in Fig. 4, comparing with those calculated from the Schrödinger-Poisson system. The spurious profile arising in the boundary layer of a MOSFET is suppressed. The new scheme provides a high resolution of carrier transport simulations with quantum confinement effects subject to the boundary conditions given by a wide range of the carrier density at the interface.

V. CONCLUSION

A new discretization scheme to the stationary QDD equation has been constructed by developing an exponential-fitting

method with the slope limiter in a class of conservative schemes. The low-order and high-order schemes to the QDD equation are produced automatically. This method can be reinterpreted as the flux-limiter method that hybridizes a low-order flux and a high-order flux into a single numerical flux. The discretization method provides good approximations to the density profile in the smooth regions and boundary layers of the electron flow and hence the new scheme allows high resolution of carrier transport simulations with quantum confinement effects in ultrasmall MOSFETs.

ACKNOWLEDGMENT

The author would like to thank Prof. T. Nogi, Kyoto University, and Prof. A. Matsumura, Osaka University, for valuable discussions.

REFERENCES

- [1] S. E. Laux and F. Stern, "Electron states in narrow gate-induced channels in Si," *Appl. Phys. Lett.*, vol. 49, no. 2, pp. 91–93, Jul. 1986.
- [2] K. Uchida, H. Watanabe, A. Kinoshita, J. Koga, T. Numata, and S. Takagi, "Experimental study on carrier transport mechanisms in ultrathin-body SOI n- and p-MOSFETs with SOI thickness less than 5 nm," in *IEDM Tech. Dig.*, Dec. 2002, pp. 47–50.
- [3] M. G. Ancona and G. J. Iafrate, "Quantum correction to the equation of state of an electron gas in a semiconductor," *Phys. Rev. B, Condens. Matter*, vol. 39, no. 13, pp. 9536–9540, May 1989.
- [4] C. L. Gardner, "The quantum hydrodynamic model for semiconductor devices," *SIAM J. Appl. Math.*, vol. 54, no. 2, pp. 409–427, 1994.
- [5] M. G. Ancona and B. A. Biegel, "Nonlinear discretization scheme for the density gradient equations," in *Proc. SISPAD*, Sep. 2000, pp. 196–199.
- [6] M. G. Ancona, "Finite-difference schemes for the density gradient equations," *J. Comput. Electron.*, vol. 1, no. 3, pp. 435–443, Oct. 2002.
- [7] S. Odanaka, "Multidimensional discretization of the stationary quantum drift–diffusion model in ultra-small MOSFET structures," *IEEE Trans. Comput.-Aided Design Integr. Circuits Syst.*, vol. 23, no. 6, pp. 837–842, Jun. 2004.
- [8] T.-W. Tang, X. Wang, and Y. Li, "Discretization scheme for the density-gradient equation and effect of boundary conditions," *J. Comput. Electron.*, vol. 1, no. 3, pp. 389–393, Oct. 2002.
- [9] M. G. Ancona and H. F. Tiersten, "Macroscopic physics of the silicon inversion layer," *Phys. Rev. B, Condens. Matter*, vol. 35, no. 15, pp. 7959–7965, 1987.
- [10] D. K. Ferry and J.-R. Zhou, "Form of the quantum potential for use in hydrodynamic equations for semiconductor device modeling," *Phys. Rev. B, Condens. Matter*, vol. 48, no. 11, pp. 7944–7950, 1993.
- [11] G. I. Marchuk, *Methods of Numerical Mathematics*. New York: Springer-Verlag, 1982.
- [12] D. L. Scharfetter and H. K. Gummel, "Large signal analysis of a silicon read diode oscillator," *IEEE Trans. Electron Devices*, vol. 16, no. 1, pp. 64–77, Jan. 1969.
- [13] R. J. LeVeque, *Numerical Methods for Conservation Laws*. Boston, MA: Birkhäuser, 1992.



Shinji Odanaka (M'98–SM'01) received the B.S., M.S., and Ph.D. degrees in applied mathematics and physics from Kyoto University, Kyoto, Japan, in 1978, 1980, and 1991, respectively.

From 1980 to 2000, he conducted research on semiconductor process and device modeling, computer-aided design for CMOS VLSI technologies, and CMOS devices at Matsushita Electric Industrial Co., Ltd., Osaka, Japan. He pioneered three-dimensional models for numerical process simulation in the silicon/oxide system and developed

a three-dimensional CAD model for integrated circuit processes and devices, using a supercomputer. In 2000, he joined the Cybermedia Center, Osaka University, Osaka, where he is currently a Professor with the Computer Assisted Science Division. His research interests include numerical and mathematical modeling of semiconductor transport.

Dr. Odanaka is a member of the Institute of Electronics, Information and Communication Engineers of Japan and the Japan Society of Applied Physics. He served on several program committees of the International Electron Device Meeting from 1992 to 1993, the Symposium on VLSI Technology from 1995 to 1999, and SISPAD.